Published in IET Renewable Power Generation
Received on 29th June 2013
Revised on 31st January 2014
Accepted on 26th March 2014
doi: 10.1049/iet-rpg.2013.0199

ISSN 1752-1416

Reactive power control for voltage stability of standalone hybrid wind–diesel power system based on functional model predictive control

Ahmed M. Kassem[1], *Almoataz Y. Abdelaziz*[2]

[1]*Electrical Department, Beni Suef University, Beni Suef, Egypt*
[2]*Department of Electrical Power and Machines, Faculty of Engineering, Ain Shams University, Cairo, Egypt*
E-mail: Kassem_ahmed53@hotmail.com

Abstract: This study investigates the application of the model predictive control (MPC) approach for voltage stability of an isolated hybrid wind–diesel generation system based on reactive power control. This scheme consists of a synchronous generator (SG) for a diesel-generator (DG) system and an induction generator (IG) for a wind energy conversion system. A static voltage automatic regulator (VAR) compensator (SVC) is connected at terminal bus to stabilise load voltage through compensating of reactive power. Two control paths are used to stabilise load bus voltage based on MPC. The first one by controlling the total reactive power of the system that by controlling the SVC firing angle and hence the load voltage. The second control path by controlling the SG excitation voltage and hence the load bus terminal voltage. The MPC is used to determine the optimal control actions including system constraints. To mitigate calculations effort and to reduce numerical problems, especially in large prediction horizon, an exponentially weighted functional MPC (FMPC) is applied. The proposed controller has been tested through step change in load reactive power plus step increase in input wind power. Also, the performance of the system with FMPC was compared with the classical MPC. Moreover, this scheme is tested against the parameters variations.

Nomenclature

E_{m}	electromagnetic energy stored in induction generator (IG)
ΔE_{m}	small signal in the electromagnetic energy stored in induction generator (IG)
ΔE_{fd}, ΔE_q, $\Delta E'_q$	small change in the voltages of the exciter, internal armature under steady state and transient conditions, respectively
K_F, K_α	voltage stabiliser and thyristor-firing gain constants, respectively
Q_{IG}	reactive power needed by IG
P_{IW}	the real power input by the IG
Q_{SG}	reactive power supplied by a diesel generator (DG)
Q_{SVC}	reactive power generated by SVC
Q_{L}	reactive-power-load demand
B_{SVC}	reactive susceptance of the SVC
D_V	load voltage characteristics
E_q	the synchronous generator armature EMF under steady state condition
T_α	Thyristor-firing delay time
T_d	SVC average dead time of zero crossing in a three-phase system
α, α_o	Thyristor controlled reactor (TCR) firing angle and its nominal value, respectively
δ	power angle between terminal voltage and armature internal EMF
R_1, X_1, R'_2, X'_2	stator resistance, stator reactance, rotor resistance, and rotor reactance referred to the primary side of IG, respectively
$R_{\mathrm{equ}}, X_{\mathrm{equ}}$, X_{m}	equivalent resistance, equivalent reactance, and magnetising reactance of the IG, respectively
T_F, T_R	stabiliser, and regulator time constants, respectively
T'_{do}	direct-axis open-circuit transient time constant
V_t	bus terminal voltage
V_{t}^o	nominal value of bus terminal voltage
ΔV_{t}, ΔV_{ref}, ΔV_{a}, ΔV_{f}	small change in the voltages of terminal voltage, reference voltage, amplifier output voltage, and exciter feedback voltage, respectively
x_d, x'_d	direct-axis reactance of synchronous generator (SG) under steady-state and transient-state conditions, respectively
Q_{c}	rating of the SVC

Q_R	system reactive-power rating
N_p	prediction horizon
N_c	control horizon
σ	tuning parameter in exponential data weighting
μ_k and v_k	the weighting factors for the prediction error and control energy, respectively
t_s	settling time
MOS	maximum overshoot
SVC	static VAR compensator
MPC	model predictive control
GPC	generalised predictive control
RHC	receding horizon control
IG	induction generator
FMPC	functional model predictive control

1 Introduction

During last few decades, the potential assessment of the sustainable eco-friendly power sources and the technology refinement has taken place so that economical and reliable power can be produced. Different renewable sources are available at different geographical locations close to loads, therefore the latest trend is to have distributed or dispersed power system. Example of such systems is wind–diesel. This system is known as hybrid power systems [1–5]. The advantage of hybrid power systems is the combination of the continuously available as diesel power generation and locally available, non-polluting as wind energy. Also, using such hybrid power system can decrease both the annual diesel fuel consumption and the level of pollution.

Normally, in hybrid generation systems, there is more than one type of electrical generators [6–10]. In general, synchronous generators are used with diesel generation system and induction generators are used with wind generation systems [11]. Induction generators have some advantages over a synchronous generators especially as a source of standalone power generation as decreased unit cost, ease of maintenance, ruggedness, brushless and no need of using external dc source [12–14]. The main disadvantage of induction generator is that it needs a reactive power for its operation. In case of grid connected system, induction generator can obtain the required reactive power from the grid or from a capacitor bank, whereas in case of a standalone system, reactive power can only be produced by capacitor banks and/or synchronous generator. The mismatch in consumption and generation of the reactive power can cause a seriously problem of voltage fluctuations at generator terminals. Hence, in case of isolated hybrid wind–diesel generation system, a reactive power device with a suitable regulator is needed to maintain the voltage within the specified limits and to avoid the voltage instability.

Recently, there is a great require a strategy to improve the reactive-power-control strategy of the standalone hybrid power generation to maintain the voltage within the specified limits. Static VAR compensator (SVC) is the one of the commonly reactive power device used in power system [15–20]. The main reason of using the SVC is to stabilise the terminal voltage of the power systems. In case of isolated hybrid power system, both the induction generator and the load obtain their variable needed reactive power from only the reactive power device. In the absence of suitable reactive device and controls, the system can be subjected to voltage instability. Many control strategies are applied to control the reactive power generated by SVC that by controlling the thyristor firing angle as state feedback control [21], neural network control [22] and model predictive control (MPC) [23].

In recent years, A lot of literatures have been applied MPC in energy conversion [23–26]. The model predictive controller normally needs a significant computational effort. As the performance of the available computing hardware has fast increased and new rapid algorithms have been presented, it is now possible to apply MPC to command rapid systems with small time steps, as electrical machines. Electric machines have particular interest for using MPC for at least the following two reasons [27, 28]:

1. They fit in the type of systems for which a quite good linear model can be obtained by analytical means and identification approaches;
2. Anti-windup approach is the main technique to deal with system constraints, which widely is used in MPC.

To overcome the voltage instability in isolated hybrid wind–diesel power system, an automatic reactive power control based on SVC and MPC with large prediction horizon is presented in this study. This proposed scheme is similar to automatic generation control. The main challenge of MPC for centralised hybrid wind–diesel power system is its large computational effort required. To overcome this drawback, a functional MPC with orthonormal basis Laguerre function is proposed [29]. The presented functional MPC decreases computational effort significantly which makes it more appropriate for applicable implementation. Also, an exponential data weighting is used to decrease numerical issue in MPC with large prediction horizon [30].

The system state equations have been obtained with transfer-function block-diagram representation of the control system. The voltage deviation error is used as the reactive-power-control input to eliminate the reactive-power incompatibility in the system. The mathematical model of the proposed hybrid wind–diesel system using reactive power flow equations is presented in Section 2. The proposed standalone hybrid wind–diesel generation system with SVC and the proposed functional MPC (FMPC) has been tested through a step change in load reactive power plus step increase in input wind power.

2 Mathematical modelling of wind–diesel system

Fig. 1 shows a standalone hybrid wind–diesel generation system. This system consists of synchronous generator driven by diesel engine, induction generator driven by wind turbine, SVC providing the required reactive power and isolated load. It is proposed that the synchronous generator with the excitation system is coupled with diesel engine. The synchronous generator-diesel system is considered as a local grid for the wind-induction generator system. Small changes in the reactive power mainly affect the voltage, while small changes in the active power essentially affect the frequency. Cross coupling between the load frequency control and the automatic voltage regulator (AVR) loop is negligible, wherever the excitation time constant is much smaller than the prime mover time constant. Under steady-state condition, the reactive power balance equation of the system can be written as following

$$\Delta Q_{SVC} + \Delta Q_{SG} = \Delta Q_{IG} + \Delta Q_{L} \quad (1)$$

doi: 10.1049/iet-rpg.2013.0199

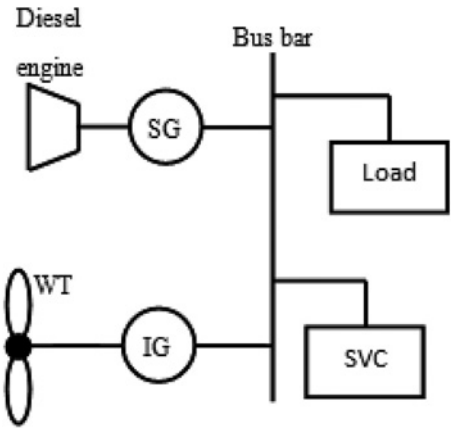

Fig. 1 *Schematic diagram of the proposed isolated hybrid wind–diesel generation system*

Assuming the proposed hybrid wind–diesel system has a reactive power load change of magnitude ΔQ_{L}. Then, the system reactive power generation increases by an amount of $\Delta Q_{\mathrm{SVC}} + \Delta Q_{\mathrm{SG}}$. Owing to the impact of the SVC and AVR controllers, the reactive power of the proposed generation system increases by an amount of $\Delta Q_{\mathrm{SVC}} + \Delta Q_{\mathrm{SG}}$. The required reactive power will also change because of the change in the voltage by ΔV_t. Then, the surplus of the reactive power in the system can be written as [11]

$$\Delta Q_{\mathrm{net}} = \Delta Q_{\mathrm{SVC}} + \Delta Q_{\mathrm{SG}} - \Delta Q_{\mathrm{IG}} - \Delta Q_{\mathrm{L}} \tag{2}$$

Increasing in net reactive power of the system will increase the system voltage that by both increasing the electromagnetic energy absorption (E_{m}) of the induction generator at rate d/dt (E_{m}) and by an increasing in the reactive load consumption of the system because of an increase in terminal voltage. This can be written using the following equation

$$\Delta Q_{\mathrm{SVC}} + \Delta Q_{\mathrm{SG}} - \Delta Q_{\mathrm{IG}} - \Delta Q_{\mathrm{L}} = \frac{\mathrm{d}\Delta E_m}{\mathrm{d}t} + D_v \Delta V_t \tag{3}$$

The stored electromagnetic energy in the induction generator

$$E_M = \frac{1}{2} L_M I_M^2 = \frac{V_t^2}{4\pi f X_M} \tag{4}$$

where I_M, L_M and X_M are the current, inductance and reactance of the induction generator, respectively, and f is the system frequency.

From (4) ΔE_M can be written as following

$$\Delta E_M = E_M - E_M^o = \frac{2E_M^o}{V^o} \Delta V_t \tag{5}$$

where E_M^o and V_t^o are the nominal values of electromagnetic energy stored in the IG and terminal voltage. With the increase in voltage, all the connected reactive-power-loads experience an increase by $D_{\mathrm{V}} = \partial Q_{\mathrm{L}} / \partial V_t$ (per unit kilovolt-amperes reactive/per unit kilovolt).

In transient condition case, Q_{SG} is given by [12, 13]

$$Q_{\mathrm{SG}} = \frac{E_q' V_t \cos\delta - V_t^2}{X_d'} \tag{6}$$

Flux linkage E_q' of the round rotor SG for small disturbance is given by [12]

$$\frac{\mathrm{d}\Delta E_q'}{\mathrm{d}t} = \frac{\Delta E_{fd} - \Delta E_q}{T_{do}'} \tag{7}$$

where ΔE_q is [12]

$$\Delta E_q = \frac{x_d}{x_d'} \Delta E_q' - \frac{x_d - x_d'}{x_d'} \cos\delta \, \Delta V_t \tag{8}$$

The load reactive power Q_{L} can be expressed in the voltage form as [12]

$$Q_{\mathrm{L}} = C_1 V_t^q \tag{9}$$

where C_1 is the constant of the load constant, and q is an exponent depends upon the load type.

For small perturbations, The load voltage characteristics D_V, can be found empirically as

$$D_V = \frac{\Delta Q_{\mathrm{L}}}{\Delta V_t} = q \frac{Q_{\mathrm{L}}^o}{V_t^o} \tag{10}$$

Where Q_{L}^o is the nominal value of the load reactive-power demand.

The reactive power given by the SVC can be written as following [12], where block diagram of SVC is shown in Fig. 2

$$Q_{\mathrm{SVC}} = B_{\mathrm{SVC}} V_t^2 \tag{11}$$

where

$$L_{\mathrm{eq}} = \frac{\pi L_o}{2(\pi - \alpha) - \sin(2\alpha)},$$

$$B_{\mathrm{SVC}} = \frac{4\pi^2 f^2 L_{\mathrm{eq}} C_o - 1}{2\pi f L_{\mathrm{eq}}}$$

α is the thyristor firing angle and f is the terminal voltage frequency.

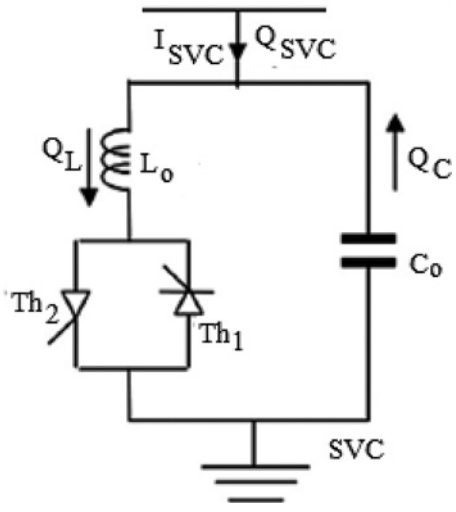

Fig. 2 *Block diagram of SVC*

Based on small changes in terms of generator terminal voltage and parameters and based on (4), the reactive power supplied by the induction generator for constant slip model is given as [11]

$$\Delta Q_{\mathrm{IG}} = \frac{2V_t^o X_{\mathrm{equ}}}{\left((1-s)R_2'/s - R_{\mathrm{equ}}\right)^2 + X_{\mathrm{equ}}^2}\Delta V_t + \frac{-2(V_t^o)^2 X_{\mathrm{equ}} R_Y}{\left\{2R_Y\left(P_{\mathrm{IW}} - P_{\mathrm{coreloss}}\right) + (V_t^o)^2\right\}\left(R_Y^2 + X_{\mathrm{equ}}^2\right)}\Delta P_{\mathrm{IW}} \tag{12}$$

where

$$R_Y = R_P - R_{\mathrm{equ}}$$

$$R_P = \frac{R_2'}{s}(1-s)$$

$$R_{\mathrm{equ}} = R_1 + R_2'$$

$$X_{\mathrm{equ}} = X_1 + X_2'$$

where approximate equivalent circuit diagram of induction generator is shown in Fig. 3.

From the SVC model shown in Fig. 4, and assuming an integral control applied, the small perturbations of thyristor firing angle α, the reactive suscepetances of the SVC B'_{SVC} and B_{SVC} can be written as following [22]

$$\frac{\mathrm{d}\Delta\alpha}{\mathrm{d}t} = \left[\Delta V_{\mathrm{ref}} - \Delta V_t\right] \tag{13}$$

$$\frac{\mathrm{d}\Delta B'_{\mathrm{SVC}}}{\mathrm{d}t} = -\frac{1}{T_\alpha}\Delta B'_{\mathrm{SVC}} + \frac{K_\alpha}{T_\alpha}\Delta\alpha \tag{14}$$

$$\frac{\mathrm{d}\Delta B_{\mathrm{SVC}}}{\mathrm{d}t} = -\frac{1}{T_d}\Delta B_{\mathrm{SVC}} + \frac{1}{T_d}\Delta B'_{\mathrm{SVC}} \tag{15}$$

The small change in synchronous generator exciter voltage ΔE_{fd}, feedback voltage ΔV_f and amplifier output voltage

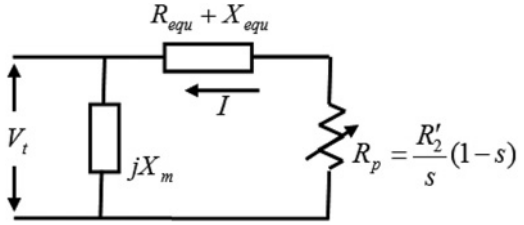

Fig. 3 *Approximate equivalent circuit diagram of induction generator*

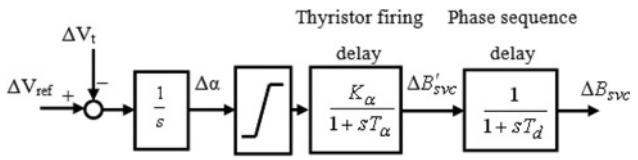

Fig. 4 *Block diagram of the proposed small-signal thyristor-controlled SVC*

ΔV_a based on the system block diagram shown in Fig. 5 can be given as following

$$\frac{\mathrm{d}\Delta E_{fd}}{\mathrm{d}t} = -\frac{K_{\mathrm{E}}}{T_{\mathrm{E}}}\Delta E_{fd} + \frac{1}{T_{\mathrm{E}}}\Delta V_a \tag{16}$$

$$\frac{\mathrm{d}\Delta V_f}{\mathrm{d}t} = \frac{K_F}{T_F T_{\mathrm{E}}}\left[\Delta V_a - K_{\mathrm{E}}\Delta E_{fd}\right] - \frac{1}{T_F}\Delta V_f \tag{17}$$

$$\frac{\mathrm{d}\Delta V_a}{\mathrm{d}t} = \Delta V_{\mathrm{ref}} - \left(\Delta V_f + \Delta V_t\right) \tag{18}$$

2.1 System complete model

By controlling of the proposed hybrid generation system net reactive power, the load terminal amplitude voltage can be stabilised. Using equations. (4)–(18) and the system block diagram shown in Fig. 5, the complete linearised mathematical model of the system in case of small perturbation can be written as following

$$\frac{\mathrm{d}\Delta E_{fd}}{\mathrm{d}t} = -\frac{K_{\mathrm{E}}}{T_{\mathrm{E}}}\Delta E_{fd} + \frac{1}{T_{\mathrm{E}}}\Delta V_a \tag{19}$$

$$\frac{\mathrm{d}\Delta V_a}{\mathrm{d}t} = \Delta V_{\mathrm{ref}} - \left(\Delta V_f + \Delta V_t\right) \tag{20}$$

$$\frac{\mathrm{d}\Delta V_f}{\mathrm{d}t} = \frac{K_{\mathrm{F}}}{T_{\mathrm{F}} T_{\mathrm{E}}}\left[\Delta V_a - K_{\mathrm{E}}\Delta E_{fd}\right] - \frac{1}{T_{\mathrm{F}}}\Delta V_f \tag{21}$$

$$\frac{\mathrm{d}\Delta E'_q}{\mathrm{d}t} = \frac{K_1}{T_G}\Delta E_{fd} - \frac{1}{T_G}\Delta E'_q + \frac{K_2}{T_G}\Delta V_t \tag{22}$$

$$\frac{\mathrm{d}\Delta B_{\mathrm{SVC}}}{\mathrm{d}t} = -\frac{1}{T_d}\Delta B_{\mathrm{SVC}} + \frac{1}{T_d}\Delta B'_{\mathrm{SVC}} \tag{23}$$

$$\frac{\mathrm{d}\Delta B'_{\mathrm{SVC}}}{\mathrm{d}t} = -\frac{1}{T_\alpha}\Delta B'_{\mathrm{SVC}} + \frac{K_\alpha}{T_\alpha}\Delta\alpha \tag{24}$$

$$\frac{\mathrm{d}\Delta\alpha}{\mathrm{d}t} = \left[\Delta V_{\mathrm{ref}} - \Delta V_t\right] \tag{25}$$

$$\frac{\mathrm{d}\Delta V_t}{\mathrm{d}t} = \frac{K_3 K_V}{T_V}\Delta E'_q + \frac{K_7 K_V}{T_V}\Delta B_{\mathrm{SVC}} + \frac{K_V K_4 + K_V K_6 - K_V K_5 - 1}{T_V} \times \Delta V_t - \frac{1}{T_V}\Delta Q_{\mathrm{L}} - K_8\Delta Q_{\mathrm{IW}} \tag{26}$$

Then, the state space model of the reactive power control of the hybrid wind–diesel generation system using (19)–(26) can be written as following

$$\dot{x} = Ax + Bu + Ed \tag{27}$$

where x is the state vector, u is the control input vector and d is the disturbance vector, where

$$\boldsymbol{x} = \left[\boldsymbol{\Delta E}_{fd}\ \boldsymbol{\Delta V}_f\ \boldsymbol{\Delta V}_a\ \boldsymbol{\Delta E}'_q\ \boldsymbol{\Delta B}_{\mathrm{SVC}}\ \boldsymbol{\Delta B}'_{\mathrm{SVC}}\ \boldsymbol{\Delta\alpha}\ \boldsymbol{\Delta V}_t\right]$$

$$\boldsymbol{u} = \left[\boldsymbol{\Delta V}_{\mathrm{ref}}\right]$$

$$\boldsymbol{d} = \left[\boldsymbol{\Delta Q}_{\mathrm{L}}\ \ \boldsymbol{\Delta P}_{\mathrm{IW}}\right]$$

The synchronous generator, induction generator, SVC and

doi: 10.1049/iet-rpg.2013.0199

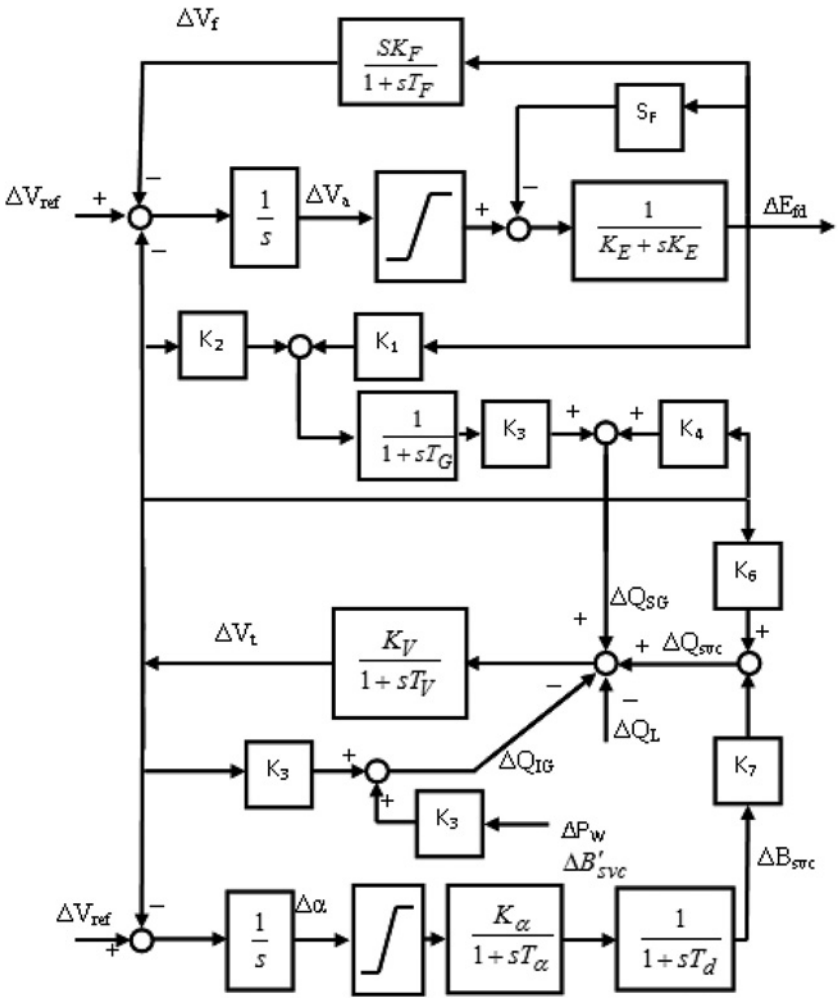

Fig. 5 *Transfer function block diagram of the hybrid wind–diesel system*

load parameters are shown in Appendix 1. Also, the system constants are presented in Appendix 2.

3 Functional model predictive control

3.1 Model predictive Control

Generally, MPC uses an outright model to predict future trajectory of the states and outputs of a system. This can allow solving online optimal control problem, where control input and prediction error actions are minimised through a future horizon, possibility of subject to constraints on the manipulated inputs, outputs and states. The optimisation returns an optimal control sequence as input and the first input only from the sequence is used as input to the system. By the next sample interval, the total optimisation approach repeated and the horizon shifted. This approach (receding horizon control) is used to allow indemnity for modeling error and future disturbance.

Fig. 6 shows the basic structure of MPC. To predict future output response chain $\hat{y}$, an exact model of the system is used. Then, the error can be calculated using the current of both the

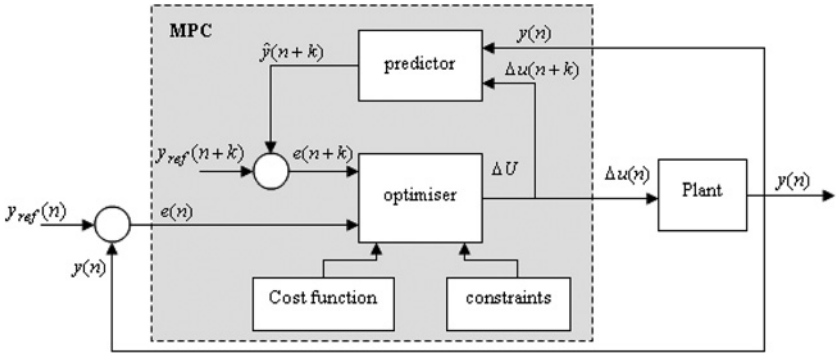

Fig. 6 *Basic structure of MPC*

system and the predicted system outputs. After that, The errors are fed to the optimiser. The future optimised control sequence, Δu, is calculated using the system constraints and objective function in the optimiser.

In this study, MPC is used the system state space model. The general form of the discrete state space model used in MPC is as following

$$\begin{aligned} x(k+1) &= Ax(k) + Bu(k) \\ &\quad + Ed(k) + Fw(k) \\ y(k) &= Cx(k) \end{aligned} \tag{28}$$

where, x is the vector of states, u is the control input vector, d is the system disturbances, w is the system noise and k is the sampling instant. A, B, C, E and F are defined as the coefficients of state space model of the system and reflect the hybrid wind–diesel generation system model in (27).

Then, main target of MPC is to reach zero output error with minimal control effort.

Therefore the cost function J which reflects the control objectives can be written as following

$$J(n) = \sum_{k=1}^{N_p} \mu_k \left(y'(n+k) - y_{ref}(n+k)\right)^2 + \sum_{k=1}^{N_c} v_k \Delta u(n+k)^2 \tag{29}$$

where

μ_k and v_k, respectively, the weighting factors for the prediction error and control energy;

$y'(n+k)$ kth step output prediction;

$y_{ref}(n+k)$ kth step reference trajectory;

$\Delta u(n+k)$ kth step control action.

Where, $1 \times N_p$ is the dimension of the predicted output vector and N_p is the prediction horizon. Δu is the control action vector with dimension of $1 \times N_c$ where N_c is the control horizon. In the MPC, N_c is always smaller than or equal to N_p. μ_k and v_k are reflecting the weights on the predicted change in the control action and error of predicted outputs, respectively.

The following are the MPC constraints include magnitude and change of input, state variables and output variables

$$\begin{aligned} &u_{min} \le u(n+k) \le u_{max}, \quad \Delta u_{min} \le \Delta u(n+k) \le \Delta u_{max} \\ &x_{min} \le x(n+k) \le x_{max}, \quad \Delta x_{min} \le \Delta x(n+k) \le \Delta x_{max} \\ &y_{min} \le y(n+k) \le y_{max}, \quad \Delta y_{min} \le \Delta y(n+k) \le \Delta y_{max} \end{aligned} \tag{30}$$

The optimal input control sequence is given by solving the objective function (29) with system constraint (30).

3.2 Laguerre based MPC

In the conventional MPC, the future control signal is considered as a vector of forward shift operator with length of N_c

$$\Delta U = \left[\Delta u(n), \ \ldots, \Delta u(n+k), \ \ldots, \Delta u(n+N_c-1)\right] \tag{31}$$

N_c is the unknown control variable which is achieved in the optimisation procedure. To achieve good closed loop performance, large prediction horizon is required, which leads to large computational burden. Therefore MPC may not be fast enough to be used as a real time optimal control for such case.

To solve this drawback, functional MPC is used. In the FMPC, future input is supposed to be a linear composition of a few simple rule functions. These can be any suitable functions. However in practical, a polynomial basis is often used [23]. Proper selection of the base function leads to more accurate of this approximation input trajectory. Hence, the term used in the optimisation procedure required by classical MPC can be reduced to fraction by using functional MPC. Therefore the load computational can be reduced strongly.

In this study, input trajectory is modelled using orthonormal basis of Laguerre function. z-transform of m'th Laguerre function can be written as following

$$\Gamma_m = \frac{\sqrt{1-a^2}}{z-a}\left[\frac{1-az}{z-a}\right]^{m-1} \tag{32}$$

where $0 \le a \le 1$ is the pole of Laguerre function. The control input sequence can be expressed by the following Laguerre functions

$$\Delta u(n+k) \simeq \sum_{m=1}^{N} c_m l_m(k) \tag{33}$$

where l_m is the z-transform inverse of Γ_m in the discrete domain, c_m is unknown coefficient and should be obtained during optimisation procedure. a and N are tuning parameters and are adjusted by the control designer. Value of N is often chosen smaller than 10, where it is sufficient for most practical applications. Also, larger value of N will increase the accuracy of input sequence estimation.

3.3 Exponentially weighted MPC

The value of prediction horizon N_p has a great effect in MPC Performance. However, increasing of N_p value will improve the system closed loop performance. However, selecting of larger value of prediction horizon is limited by numerical issue, which needs high sampling rate. Hence, MPC with Exponential data weighting can be used to be a solution of this drawback [30].

3.4 Design of the proposed FMPC

In this section, a combination of Laguerre based MPC and exponentially weighted MPC are used to alleviate computational effort and decrease numerical problems. At first, a discrete MPC with exponential data weighting is designed. Hence, input, state and output vectors are changed as following

$$\begin{aligned} \Delta \hat{U}^T &= \left[\sigma^{-0}\Delta u(n), \ \ldots, \sigma^{-(N_c-1)}\Delta u(n+N_c-1)\right] \\ \hat{X}^T &= \left[\sigma^{-1}x(n+1), \ \ldots, \sigma^{-N_p}x(n+N_p)\right] \\ \hat{Y}^T &= \left[\sigma^{-1}y(n+1), \ \ldots, \sigma^{-N_p}x(n+N_p)\right] \end{aligned} \tag{34}$$

where σ is a tuning parameter in exponential data weighting and it is larger than 1. Then, the system state space

doi: 10.1049/iet-rpg.2013.0199

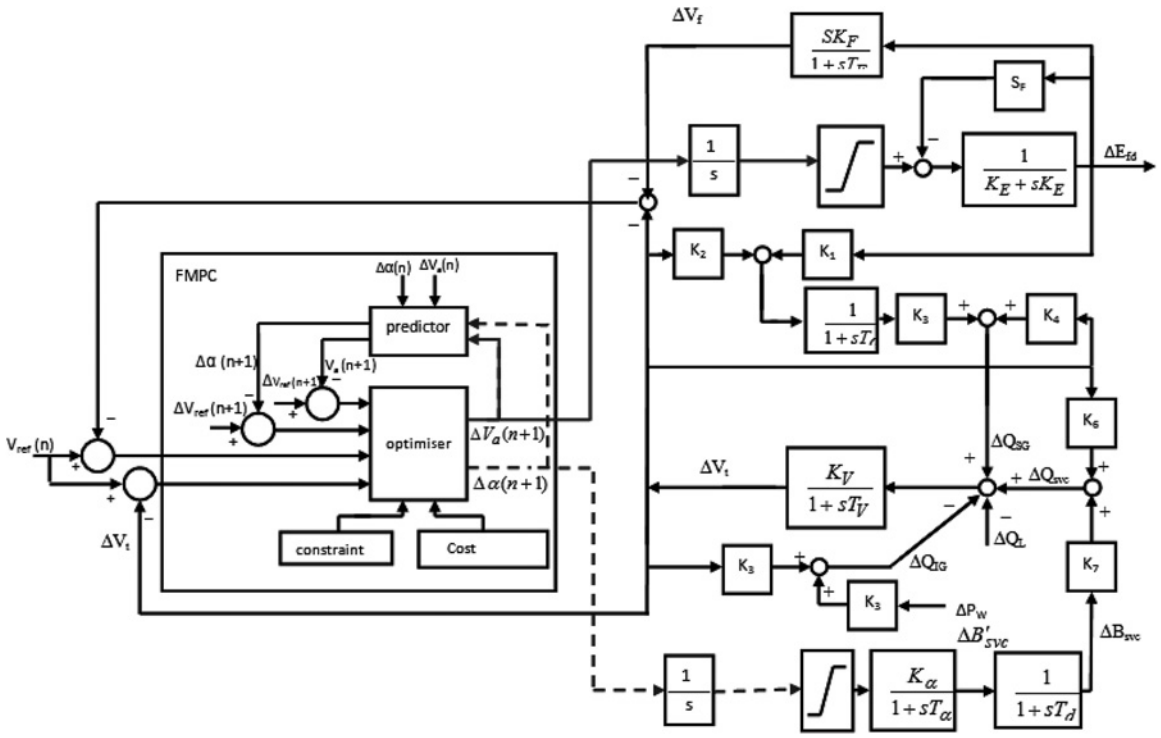

Fig. 7 *Block diagram of the wind energy conversion system with the proposed FMPC controller*

representation with transformed variable can be written as following

$$\begin{aligned}\hat{x}(n+1) &= \hat{A}\hat{x}(n) + \hat{B}\Delta\hat{u}(n)\\ \hat{y}(n) &= \hat{C}\hat{x}(n)\end{aligned} \tag{35}$$

where $\hat{A} = A/\sigma$, $\hat{B} = B/\sigma$, $\hat{C} = C/\sigma$.

By solving the above new objective function and constraints, optimal control trajectory with transformed variables can be achieved

$$\hat{J}(n) = \sum_{k=1}^{N_p} \mu_k \left(\hat{y}(n+k) - y_{ref}(n+k)\right)^2 + \sum_{k=1}^{N_c} v_k \Delta\hat{u}(n+k)^2 \tag{36}$$

$$\begin{aligned}\sigma^{-k}u_{min} \le \hat{u}(n+k) \le \sigma^{-k}u_{max},\\ \sigma^{-k}\Delta u_{min} \le \Delta\hat{u}(n+k) \le \sigma^{-k}\Delta u_{max}\\ \sigma^{-k}x_{min} \le \hat{x}(n+k) \le \sigma^{-k}x_{max},\\ \sigma^{-k}\Delta x_{min} \le \Delta\hat{x}(n+k) \le \sigma^{-k}\Delta x_{max}\\ \sigma^{-k}y_{min} \le \hat{y}(n+k) \le \sigma^{-k}y_{max},\\ \sigma^{-k}\Delta y_{min} \le \Delta\hat{y}(n+k) \le \sigma^{-k}\Delta y_{max}\end{aligned} \tag{37}$$

By choosing $a > 1$, this leads to a more reliable numerical approach, where the condition number of hessian matrix will be decreased significantly, especially for large values of N_p.

After solving the above new objective function with the new variables, the obtained input trajectory should be transformed into standard variable as shown in the following equation

$$\Delta U^T = \left[a^o\Delta\hat{u}(k),\ \ldots,\ a^{(N_{c-1})}\Delta\hat{u}(k+N_c-1)\right] \tag{38}$$

The following systematic procedure can be used to combine laguerre based MPC and exponentially weighted MPC:

– Choosing the proper tuning parameter σ.
– The system parameters (A, B, C) and the system variables (U, X, Y) are transformed based on (34) and (35).
– Creating the objective function with its constraints using (37) and (38).
– Optimising the objective function based on Laguerre polynomial and then obtaining the unknown Laguerre parameters.
– Obtaining input chain based on (33).

Finally, transforming the calculated weighted input chain to unweighted input chain based on (37) and applied on the system.

Table 1 Proposed hybrid wind–diesel parameters

Synchronous generator	
K_1	0.15
K_2	0.79
K_3	6.22
K_4	–7.358
K_5	0.126
K_6	1.478
K_7	1.0
K_8	0.444
K_V	1.0
T_V	0.000106 s

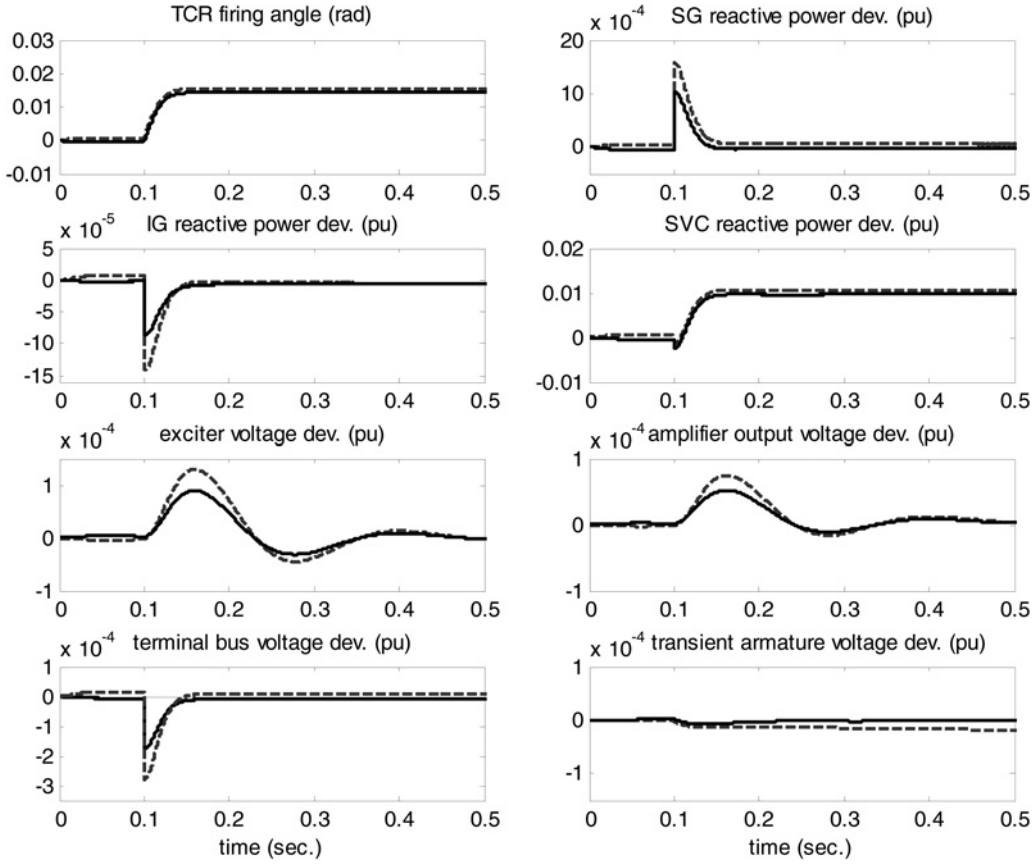

Fig. 8 *Simulation results of the proposed scheme with 1% step increase in load reactive power, with no change in input wind power, (— FMPC and - - - MPC)*

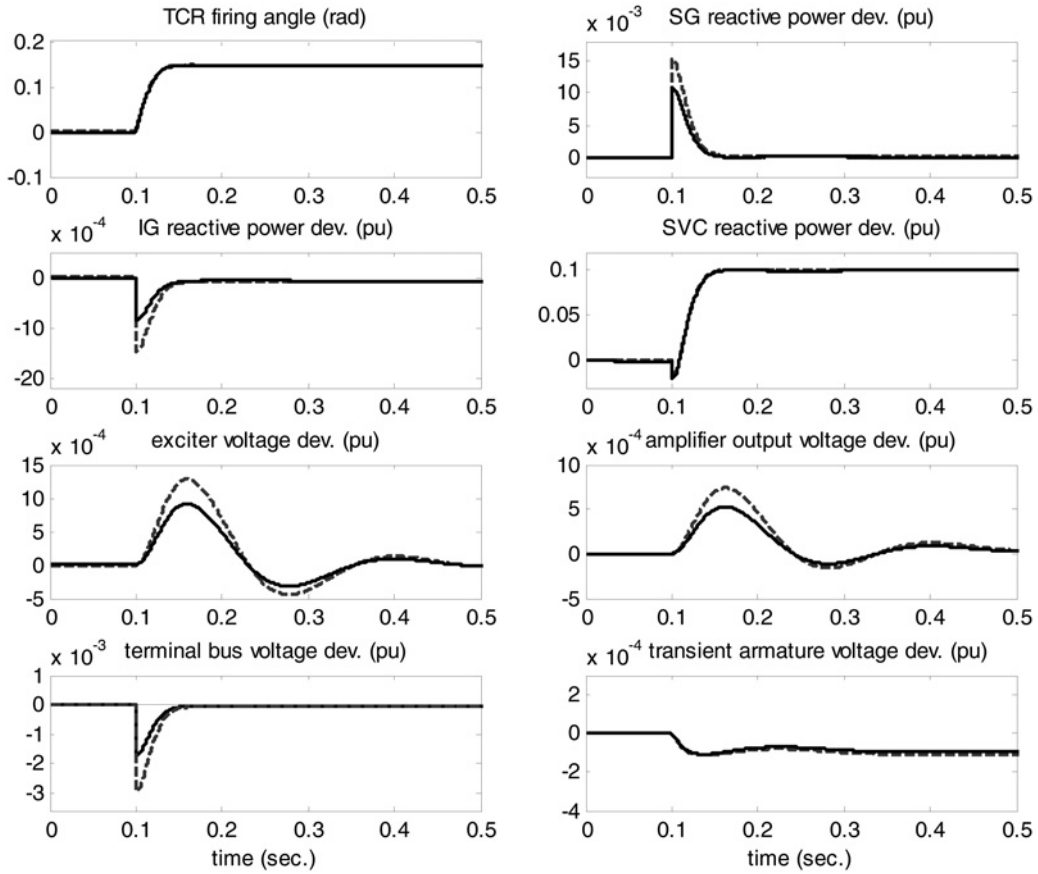

Fig. 9 *Simulation results of the proposed scheme with 10% step increase in load reactive power, with no change in input wind power, (— FMPC and - - - MPC)*

doi: 10.1049/iet-rpg.2013.0199

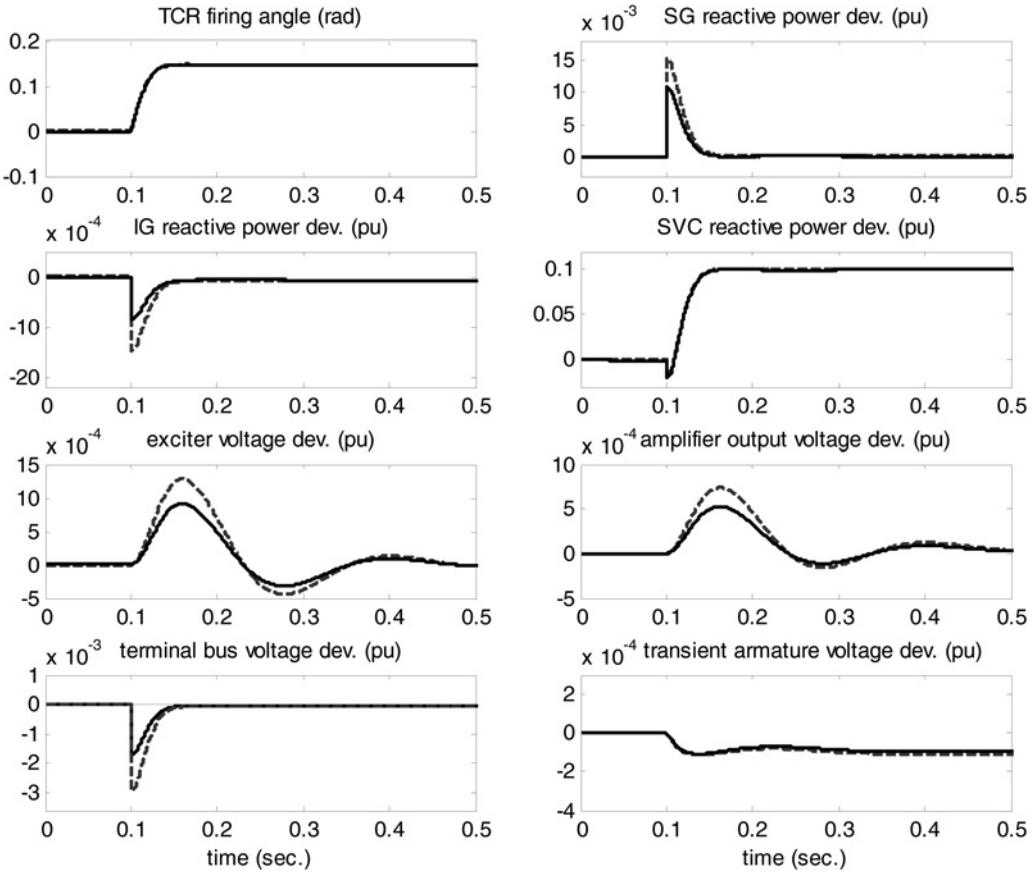

Fig. 10 *Simulation results of the proposed scheme with 10% step change in load reactive power with no change in input wind power, (— FMPC and - - - MPC)*

The main difference between the functional MPC and the classical MPC can be summarised as follows:

– In case of functional MPC, the initial control input sequence $\Delta\hat{u}(n+k)$ is generated based on Laguerre function and the exponentially weights as described by (32) and (33). Then, the initial control input sequence is used to obtain the optimal control trajectory by minimising the cost function J shown in (36). Using the initial control input sequence with suitable weighting factors, μ_k and v_k decrease the computational burden necessary for obtaining the optimal control trajectory.
– In case of classical MPC, the optimal control trajectory $\Delta u(n+k)$ is obtained directly by minimising the cost function J shown in (29). In this case, more calculations are needed to minimise the cost function J such that the optimal control trajectory can be obtained.

Table 2 Comparison between the proposed FMPC and the classical MPC

	FMPC		classical MPC	
	t_s, s	MOS, p.u	t_s, s	MOS, p.u
10% load reactive power change	0.03	-1.8×10^{-3}	0.03	-3×10^{-3}
10% load and 10% wind power change	0.035	-3.8×10^{-3}	0.04	-7.3×10^{-3}

– Therefore in case of classical MPC larger values of prediction horizon and control horizon are needed to obtain optimal control trajectory that give the desired system performance. Note that lager values of prediction horizon and control horizon will increase the computational burden. In case of functional MPC small values of prediction horizon and control horizon can obtain optimal control signal compared with the lager values needed by the classical MPC.

4 System configuration

Generally, Induction generator needs reactive power for its operation. In case of autonomous hybrid power system, the induction generator can obtain its needed reactive power only by synchronous generator/capacitor banks. The mismatch in consumption and generation of the reactive power causes a serious problem of large voltage fluctuations at generator terminals (voltage instability). Hence, there is a great need to improve the reactive power control strategy of the standalone hybrid power system to maintain the voltage within the specified limits and avoid the voltage instability.

In this study, a reactive power control based on SVC and functional MPC is presented to overcome this problem of voltage instability.

Fig. 7 shows the block diagram of the isolated hybrid wind–diesel system with the FMPC controller. Two different paths of control are applied here based on functional MPC to stabilise load bus voltage. The first path is dedicated for regulating the load bus voltage to a

reference value by adjusting the thyristor firing angle of the SVC. The second path is used to control the synchronous generator's terminal voltage to a reference value and hence the load bus voltage via controlling the excitation voltage of the synchronous generator.

Digital simulations are obtained to validate the performance of the FMPC with the isolated hybrid wind–diesel generation system. The input to the FMPC is the terminal voltage error, whereas the output of the FMPC are considered as the firing angle of the SVC, $\Delta\alpha$ and the input voltage of synchronous generator excitation system, ΔV_a. The control parameters are assumed as following

input weight matrix: $\mu = 0.15 \times I_{Nc \times Nc}$
output weight matrix: $v = 1 \times I_{Np \times Np}$

The constraints are chosen such that, the SVC firing angle α is normalised to be between 0 and 1, where 0 corresponds to ($\alpha_{\min}$) and 1 corresponds to maximum firing angle ($\alpha_{\max}$). Also, the excitation input voltage V_a is normalised to be between 0 and 1, where 0 corresponds to $V_{a(\min)} = 0$ and 1 corresponds to maximum excitation input voltage ($V_{a(\max)}$), thus

$$\begin{bmatrix} \alpha_{\min} \\ V_{a(\min)} \end{bmatrix} = 0 \le u \le 1 = \begin{bmatrix} \alpha_{\max} \\ V_{a(\max)} \end{bmatrix}$$

The constraints on the states are chosen such that to guarantee signals stay at physically reasonable values and do not grow increased steadily and that makes the control to avoid saturation effect as follows

$$x_{\min} = (0) \le \begin{pmatrix} \begin{vmatrix} V_f \\ V_a \\ E'_q \\ V_t \end{vmatrix} \end{pmatrix} \le (0.1) = x_{\max}$$

The entire system has been simulated on the digital computer using the Matlab/Simulink/software package. The parameters of the proposed system are listed in appendix [12].

5 Simulation results

Simulation results have been carried out to validate the effectiveness of the proposed system with step change in load reactive power. The parameters of the FMPC based on Laguerre function are adjusted to be $a = 0.18$, $N = 8$, $\sigma = 1.06$, $N_p = 300$ and $N_c = 8$, whereas the parameters of the classical MPC are adjusted to be $N_p = 300$ and $N_c = 9$. The performance of the proposed system with both FMPC and classical MPC has been investigated with a step change in load reactive power and input wind power. The proposed system constants values (shown in Table 1) have been calculated using system parameters given in Appendix 1 and system constants equations given in Appendix 2.

Simulation results depicting the variations of different variables with wide range variations of load reactive power and input wind power. Fig. 8 shows the system variables variations for 1.0% step change in load reactive power. It has been noted that as the load reactive power increases, the firing angle of the thyristor will increase. This would result in increasing the equivalent inductance of the reactor in the

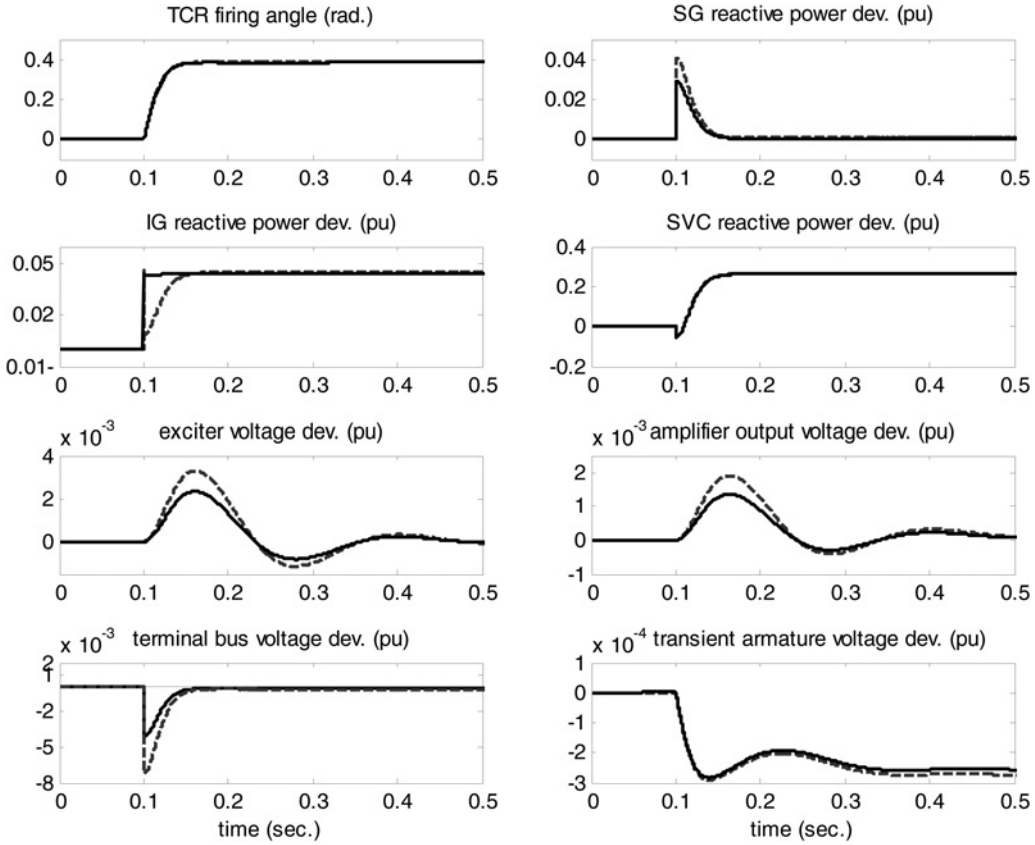

Fig. 11 *Simulation results of the proposed scheme with 15% step change in load reactive power plus 10% step increase in input wind power and parameters changes, (— FMPC and - - - MPC)*

doi: 10.1049/iet-rpg.2013.0199

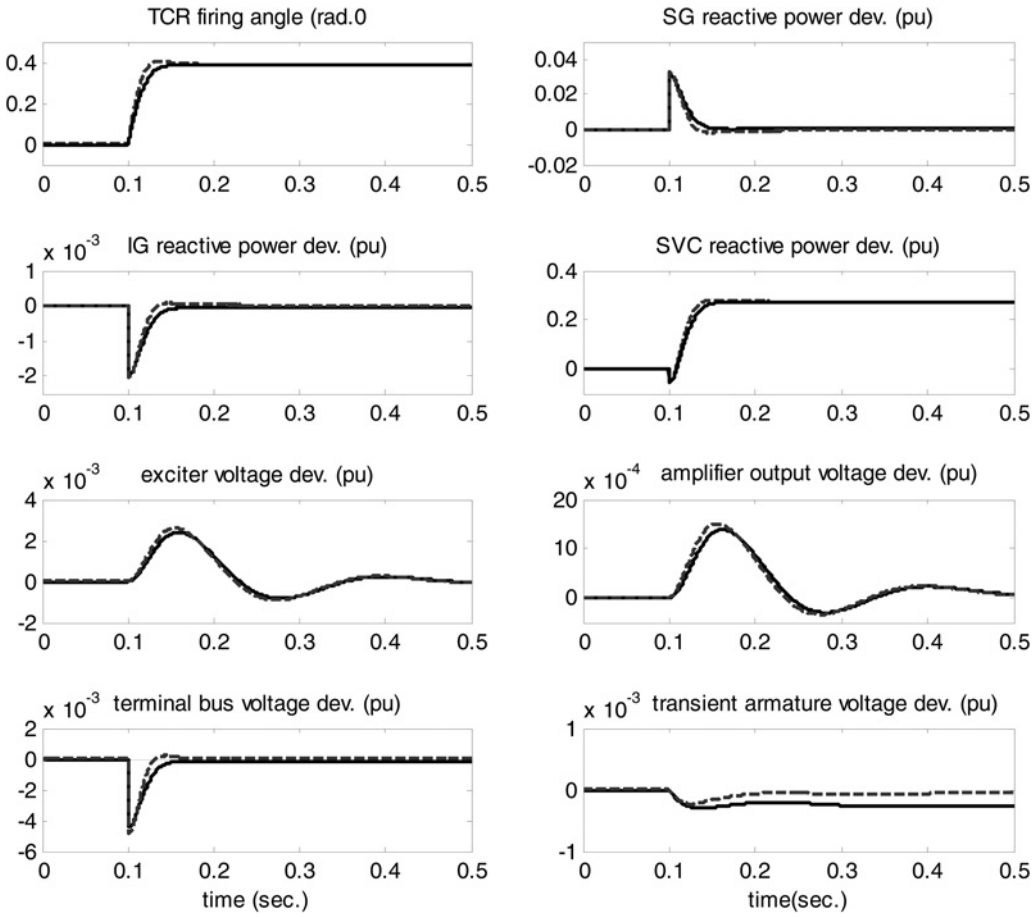

Fig. 12 *Simulation results of the proposed scheme with 15% step change in load reactive power with no change in input wind power, (— FMPC and - - - MPC)*

SVC and, in turn, decreasing the reactor current. It is also indicated that there is no steady-state error in the terminal voltage of the system with SVC and FMPC control; therefore the transient deviation in the reactive power required by the IG disappears. It is noted that the increase in the load reactive power is purely met by SVC, however the synchronous generator exciter voltage decays to zero. It also indicated that the oscillation cleared in less than 0.2 s. The deviations in the field excitation (E_{fd}) and transient armature voltage (E'_q) also follow the same trend. This figure also indicated that the FMPC has better performance than the classical MPC in case of less maximum overshoot (MOS) and settling time.

To test the controller using wide range of operating conditions, the system is tested against 10% step increase in reactive power load as shown in Fig. 9. This figure shows that the controller keep the bus terminal voltage constant at its nominal value and the transient variations are cleared in less than 0.2 s, with very-small MOS.

The dynamic responses of the isolated hybrid wind–diesel power system for 15% step increase in reactive load, plus 10% step increase in input wind power, are shown in Fig. 10. This figure shows that the increase in input wind power also increases the reactive power needed by the induction generator, and therefore fluctuations are more compared with Fig. 9, but the settling time of the response still the same because the fast action of the SVC in controlling the deviations. Also, from Figs. 8, 9 and 10 it is obvious that with the FMPC, the obtained responses of hybrid isolated wind–diesel using FMPC has less overshoot, less settling time and better response at load reactive power and input wind power changes than in case of using classical MPC. Also, Table 2 shows that in case of the FMPC the terminal bus voltage has less settling time (t_s) and less MOS than in case of classical MPC controller.

5.1 Robustness

Since our concerns are also in robust stability against various model uncertainties, some system parameters have been changed as follows:

(i) K_4 is assumed to increase by 10% above the calculated value.
(ii) K_5 is assumed to be 10% less than the calculated value.
(iii) K_6 is assumed to increase by 10% above the calculated value.

For perturbed system, the system is tested with step change of 15% increase in reactive load power plus 10% step increase in input wind power. The responses are shown in Fig. 11. It should be seen that the system is robustly stable in spite of parameters variations.

It has been indicated in the figures that the FMPC controller is able to stabilise the terminal voltage with high accuracy in spite of modelling errors and has a better performance compared with classical MPC and with elapsed simulation time of 19.952541 s in case of FMPC and 22.041603 s in case of classical MPC.

5.2 Computational burden reduction

In addition, since our concerns are in the computational burden reduction based on the proposed FMPC compared with the classical MPC, the classical MPC is tuned to improve the system performance to meet the performance of the FMPC. Therefore the prediction horizon and the control horizon are increased to be 540 and 17, respectively, while the parameters of FMPC are maintained constant as mentioned above. The system is tested with step change of 15% increase in reactive load power. The responses are shown in Fig. 12. This figure shows that both FMPC and classical MPC with high values of N_p and N_c are able to stabilise the terminal voltage with high accuracy. In this case, also the central processing unit (CPU) time is computed in both the FMPC and the classical MPC, which are found 19.952541 and 97.007168 s, respectively. These computed CPU times indicate that the FMPC can decreases the computational burden compared with the classical MPC.

6 Conclusions

This paper investigates the robust centralised functional model predictive controller for voltage stability of an isolated hybrid wind–diesel generation system considering a transfer-function model via a small signal analysis. This scheme consists of a synchronous generator driven by diesel engine, induction generator driven by wind turbine, static load and a thyristor controlled SVC. The automatic reactive-power-control model using reactive-power-flow equations have been developed for the proposed hybrid generation system. The load bus terminal voltage is stabilised by controlling both the SG excitation voltage and the firing angle of the thyristor of the SVC.

The FMPC uses orthonormal Laguerre functions to express control input trajectory, which decreases real time computation largely. Also, exponential data weighing is used to reduce numerical issue. Constraints are imposed on both the thyristor firing angle and the field excitation voltage.

Simulations results have been carried out to evaluate the effectiveness of the system. The hybrid wind–diesel generation system with the proposed controller has been tested through step change in load reactive power and input wind power. The results prove that the controller is successful in stabilising the terminal voltage of a standalone hybrid wind–diesel generation system against load and wind powers excursion and it is robust against system parameters change. Moreover, the controller has significantly better performance and less computational burden compared with classical model predictive controller.

7 References

1 Pena, R., Cardenas, R., Proboste, J., Clare, J., Asher, G.: 'Wind–diesel generation using doubly fed induction machines', *IEEE Trans. Energy Convers.*, 2008, **23**, (1), pp. 202–214

2 Sebastian, R.: 'Modeling and simulation of a high penetration wind–diesel system with battery energy storage', *Elect. Power Energy Syst.*, 2001, **33**, (3), pp. 767–774

3 Saha, T.K., Kastha, D.: 'Design optimization and dynamic performance analysis of a standalone hybrid wind–diesel electrical power generation system', *IEEE Trans. Energy Convers.*, 2010, **25**, (4), pp. 1209–1217

4 Bialasiewicz, J.T., Muljad, E., Drouilhet, S.: 'Modular simulation of a hybrid power system with diesel and wind turbine generation'. Presented at Windpower '98 Bakersfield, CA, National Renewable Energy Laboratory, 27 April–1 May, 1998

5 Ibrahim, H., Ilinca, A., Younès, R., Perron, J., Basbous, T.: 'Study of a hybrid wind–diesel system with compressed air energy storage'. IEEE Electrical Power Conf., 25–26 October 2007, pp. 320–325

6 Cardenas, R., Pena, R., Perez, M., Clare, J., Asher, G., Vargas, F.: 'Vector control of front end converters for variable speed wind–diesel systems', *IEEE Trans. Ind. Electron.*, 2006, **53**, (4), pp. 1127–1136

7 Roy, S.: 'Reduction of voltage dynamics in isolated wind–diesel units susceptible to gusting', *IEEE Trans. Sustain. Energy*, 2010, **1**, (2), pp. 84–91

8 Abbey, C., Li, W., Joos, G.: 'An online control algorithm for application of a hybrid ESS to a wind–diesel system', *IEEE Trans. Ind. Electron.*, 2010, **57**, (12), pp. 3896–3904

9 Sebastian, R.: 'Reverse power management in a wind–diesel system with a battery energy storage', *Electr. Power Energy Syst.*, 2013, **44**, (1), pp. 160–167

10 Sedaghat, B., Jalilvand, A., Noroozian, R.: 'Design of a multilevel control strategy for integration of stand-alone wind/diesel system', *Elect. Power Energy Syst.*, 2012, **35**, (1), pp. 123–137

11 Sharma, P., Bhatti, T.S.: 'Performance investigation of isolated wind–diesel hybrid power systems with WECS having PMIG', *IEEE Trans. Ind. Electron.*, 2013, **60**, (4), pp. 1630–1637

12 Bansal, R.C.: 'Automatic reactive power control of isolated wind–diesel hybrid power systems', *IEEE Trans. Ind. Electron.*, 2006, **53**, (4), pp. 1116–1126

13 Kassem, A.M., Hasaneen, K.M., Yousef, A.M.: 'Dynamic modeling and robust power control of DFIG driven by wind turbine at infinte grid', *Elect. Power Energy Syst.*, 2013, **44**, (1), pp. 375–382

14 Tandon, A.K., Murthy, S.S., Berg, G.J.: 'Steady state analysis of capacitors excited induction generators', *IEEE Trans. Power App. Syst.*, 1984, **PAS-103**, (3), pp. 612–618

15 Mathur, R.M.: 'Stabilisation techniques in power systems static VAR compensation'. Proc. IFAC Symp., Bangalore, India, December 14, 1986

16 Taylor, C.W., Scott, G., Hammad, A., *et al.*: 'Static Var compensator models for power flow and dynamic performance simulation', *IEEE Trans. Power Syst.*, 1994, **9**, (1), pp. 229–240

17 Padiyar, K.R., Verma, R.K.: 'Damping torque analysis of static VAR system controllers', *IEEE Trans. Power Syst.*, 1991, **6**, (2), pp. 458–465

18 Hammad, A.E.: 'Analysis of power system stability enhancement by static Var compensators', *IEEE Trans. Power Syst.*, 1986, **1**, (4), pp. 222–227

19 Hammad, A.E., El-Sadek, M.: 'Application of thyristor controlled Var compensator for damping sub-synchronous oscillations in power systems', *IEEE Trans. Power App. Syst.*, 1984, **PAS-103**, (1), pp. 198–212

20 Kaseem, A.M., Yousf, A.M.: 'Robust control of an isolated hybrid wind–diesel power system using linear quadratic Gaussian approach', *Elect. Power Energy Syst.*, 2011, **33**, (4), pp. 1092–1100

21 Abdin, A., Wilson, X.: 'Control design and dynamic performance analysis of a wind turbine-induction generator unit', *IEEE Trans. Energy Conver.*, 2000, **15**, (1), pp. 91–96

22 Kassem, A.M.: 'Neural control design for isolated wind generation system based on SVC and nonlinear autoregressive moving average approach', *WSEAS Trans. Syst.*, 2012, **11**, (2), pp. 39–49

23 Kassem, A.M.: 'Robust voltage control of a stand alone wind energy conversion system based on functional model predictive approach', *Elect. Power Energy Syst*, 2012, **41**, (1), pp. 124–132

24 Soliman, M., Malik, O.P., Westwick, D.T.: 'Multiple model predictive control for wind turbines with doubly fed induction generators', *IEEE Trans. Sustain. Energy*, 2011, **2**, (3), pp. 215–225

25 Muhando, E.B., Senjyu, T., Uchida, K., Kinjo, H., Funabashi, T.: 'Stochastic inequality constrained closed-loop model-based predictive control of MW-class wind generating system in the electric power supply', *IET Renew. Power Gener.*, 2010, **4**, (2), pp. 23–35

26 Zhi, D., Xu, L., William, B.W.: 'Model-based predictive direct power control of doubly fed induction generators', *IEEE Trans. on Power Electron.*, 2010, **25**, (2), pp. 341–351

27 Diab, A.A.Z., Pankratov, V.V.: 'Model predictive control of vector controlled induction motor drive'. IEEE Seventh Int. Forum on Strategic Technology (IFOST), 18–21 September 2012, pp. 1–6

28 Scoltock, J., Geyer, T., Madawala, U.K.: 'A comparison of model predictive control schemes for MV induction motor drives', *IEEE Trans. Ind. Informatics*, 2013, **9**, (2), pp. 909–919

29 Wang, L.: 'Discrete model predictive control design using Laguerre functions', *Journal of Process Control*, 2004, **14**, (2), pp. 131–142

30 Wang, L.: 'Use of exponential data weighting in model predictive control design'. Proc 40th IEEE Conf. on Decision and Control, 2001, vol. 5, pp. 4857–4862

doi: 10.1049/iet-rpg.2013.0199

8 Appendix 1: proposed hybrid wind–diesel power system parameters

Synchronous generator	
$P_{SG,}$ pu kW	0.4
Q_{SG}, pu kVAR	0.2
E_q, pu	1.11
V_t, pu	1.0
X_d, pu	1.0
X'_d, pu	0.15
T'_{do}, s	5.0
Induction generator	
$P_{IG,}$ pu kW	0.6
Q_{IG}, pu kVAR	0.189
$r_1 = r_2$, pu	0.19
$x_1 = x_2$, pu	0.56
s, pu	−4.1
Load	
$P_{L,}$ pu kW	1.0
Q_L, pu kVAR	0.75
pf (lag)	0.8
Excitation system	
K_F	0.5
T_F, s	0.715
K_E	1.0
T_E, s	0.55
S_F, s	0.0
SVC	
K_α	0.4464
T_α, s	0.005
T_d, s	0.00167
base power, kVA	250
base voltage, V	400
base impedance, Ω	21.5

Appendix 2: proposed hybrid wind–diesel power system constants

$$T_G = \frac{X'_d T'_{do}}{X_d}$$

$$T_V = \frac{2H_R}{D_V V_o}$$

$$K_V = \frac{1}{D_V}$$

$$K_1 = \frac{X'_d}{X_d}$$

$$K_2 = \frac{\left(X_d - X'_d\right)\cos\delta_o}{X_d}$$

$$K_3 = \frac{V_o \cos\delta_o}{X'_d}$$

$$K_4 = \frac{E'_{qo}\cos\delta_o}{X'_d}$$

$$K_5 = \frac{2V_o X_{\text{equ}}}{\left((1-s)R'_2/s - R_{\text{equ}}\right)^2 + X^2_{\text{equ}}}$$

$$K_6 = 2V_o B_{\text{SVC}}$$

$$K_7 = V_o^2$$

$$K_8 = \frac{-2V_o^2 X_{\text{equ}} R_Y}{\left\{2R_Y\left(P_{\text{IW}} - P_{\text{coreloss}}\right) + V_o^2\right\}\left(R_Y^2 + X^2_{\text{equ}}\right)}$$

$$R_Y = R_P - R_{\text{equ}}$$

$$R_P = \frac{R'_2}{s}(1-s)$$